On the Quasi-Three Dimensional Configuration of Magnetic Clouds

Qiang Hu[1,2] ![ORCID], **Wen He[2]**, **Jiong Qiu[3]**, **Angelos Vourlidas[4,5]** ![ORCID], **and Chunming Zhu[3]**

[1]Department of Space Science, and Center for Space Plasma and Aeronomic Research (CSPAR), The University of Alabama in Huntsville, Huntsville, AL, USA, [2]Department of Space Science, The University of Alabama in Huntsville, Huntsville, AL, USA, [3]Physics Department, Montana State University, Bozeman, MT, USA, [4]Johns Hopkins University Applied Physics Laboratory, Laurel, MD, USA, [5]IAASARS, National Observatory of Athens, Penteli, Greece

Abstract We develop an optimization approach to model the magnetic field configuration of magnetic clouds, based on a linear force-free formulation in three dimensions. Such a solution, dubbed the Freidberg solution, is kin to the axisymmetric Lundquist solution, but with more general "helical symmetry." The merit of our approach is demonstrated via its application to two case studies of in situ measured magnetic clouds. Both yield results of reduced $\chi^2 \approx 1$. Case 1 shows a winding flux rope configuration with one major polarity. Case 2 exhibits a double-helix configuration with two flux bundles winding around each other and rooted on regions of mixed polarities. This study demonstrates the three-dimensional complexity of the magnetic cloud structures.

Plain Language Summary Magnetic clouds (MCs) are a type of magnetic field structures observed in space. They possess some well-defined properties and have been well studied in the space age. The existing model for such a structure is a straight cylinder with no variation along its axis. They may impact Earth carrying significant amount of electromagnetic energy. They come in relatively large sizes. When encompassing the near-Earth space environment, their impact can last for days. MCs originate from the Sun, directly born with the so-called coronal mass ejections (CMEs) which can be seen as an ejection of large amount of solar material from telescopes aiming at the Sun. The CMEs are often accompanied by solar flares, the most energetic and explosive events in our solar system. When these happen, they release a wide range of radiations and disturbances that may adversely impact Earth with MCs being one major type of such disturbances. Therefore, studying the internal configuration of MCs is of importance to understanding their origin and impact. This study presents a more complex three-dimensional MC model to better fit the in situ spacecraft measurements of such structures, which goes beyond the current model.

1. Motivation

Magnetic clouds (MCs) are large-scale magnetic structures (usually with duration ≥ 1 day at 1 au) observed from in situ spacecraft measurements, such as those from the Advanced Composition Explorer (ACE) and Wind spacecraft in the solar wind. MCs possess three well-defined signatures in the magnetic field and plasma measurements: (1) relatively strong total magnetic field, (2) smooth rotation of one or more magnetic field components, and (3) depressed proton temperature or β value (the ratio between the thermal and magnetic pressures). The elevated magnetic field and low β value often indicate the dominance of the Lorentz force over the plasma pressure gradient and the inertia force for a magnetohydrostatic equilibrium. This leads to the force-free assumption such that the Lorentz force has to vanish. The simplest form, the linear force-free field (LFFF) formulation, has been used to model the magnetic field configuration of MCs. With one-dimensional (1D) dependence on the radial distance r from a cylindrical axis only, the LFFF model yields the well-known Lundquist solution (Lundquist, 1950), describing an axisymmetric cylindrical flux rope configuration. MCs constitute a portion of interplanetary coronal mass ejections (ICMEs). A comprehensive study of the Wind spacecraft ICME Catalogue from 1995 to 2015 revealed the nonaxisymmetric features of ICME flux ropes and called for "the development of more accurate in situ models" (Nieves-Chinchilla et al., 2018, 2019). We intend to present such a model in this Letter and will explore its wider applicability by applying to the Wind ICME Catalogue in a future study.

Besides a number of variations to the Lundquist solution (e.g., Farrugia et al., 1999; Y. Wang et al., 2016), which are mostly 1D (with r dependence only), Nieves-Chinchilla et al. (2016) proposed a sophisticated circular-cylindrical model for MCs based on a generalized radial dependence of the current density. In addition, the Grad-Shafranov (GS) reconstruction technique is able to obtain a 2D cross section of arbitrary shape of a cylindrical structure based on single-spacecraft measurements (see, Hu, 2017, for a comprehensive review). This method solves for the magnetic flux function which defines distinct flux surfaces in a 2D configuration, governed by the GS equation. The GS reconstruction was first applied to in situ observations of magnetic flux ropes by Hu and Sonnerup (2001, 2002), Hu et al. (2003, 2004). The solution yields nested flux surfaces, representing winding magnetic field lines lying on distinct cylindrical surfaces surrounding a central straight field line.

MCs are often entrained in coronal mass ejections, and sometimes associated with solar flares. Efforts have been made to relate the MC flux rope configuration with the solar source region properties. Specifically, we have carried out several investigations of comparing magnetic flux contents and field-line twist profiles in MCs with those derived from flare observations, through in situ modeling of MCs and the analysis of the magnetic reconnection sequences as manifested by the flare-ribbon brightenings in the source regions (Hu et al., 2014; Qiu et al., 2007; W. Wang et al., 2017, 2019; Zhu et al., 2020). These are largely based on highly quantitative observational analysis, with the understanding that magnetic reconnection (flare process) leads to the formation of the MC flux rope. Therefore, the magnetic topology change during the flux rope formation process on the Sun, generally in three dimensions, contributes to the complexity of the internal structure of MCs. Numerous observations and numerical studies indicate the 3D nature of flux rope configurations upon their origination on the Sun (e.g., Amari et al., 2018; Duan et al., 2019; Jiang et al., 2016; Vourlidas et al., 2013, 2014), often in the form of twisted ribbons. To account for such features, we develop an approach to probe the 3D MC field-line configuration from in situ data. An earlier attempt was made by Osherovich et al. (1999), which showed a double-helix configuration as a solution to an alternative theoretical model, but lacked rigorous applications to in situ data. That formulation takes a special form of a GS type equation, which we found to be difficult to apply to in situ spacecraft measurements. Therefore, the current approach reported here is developed to provide a new capability of modeling 3D MC structures by directly employing in situ spacecraft measurements.

In what follows, we demonstrate our approach with optimal fitting of the 3D Freidberg solution (Freidberg, 2014) to single-spacecraft measurements of MCs, strictly following the appropriate χ^2 minimization methodology (Press et al., 2007). In doing so, we intend to stimulate discussions on what defines a magnetic flux rope. As a general feature of the Freidberg solution as we reveal in the following sections, the magnetic field configuration deviates from a 2D geometry for a conventionally defined "flux rope" in that there generally does not exist a straight central field line. The field lines form flux bundles that wind along the z dimension, similar to the topological feature of writhe as described in Berger and Field (1984) and particularly by Al-Haddad et al. (2011) for MCs.

2. Method

The method we develop is based on an LFFF formulation in three dimensions, namely, in a cylindrical coordinate system (r, θ, z). The following is a direct copy of the set of equations given in Freidberg (2014), representing a series solution to the equation $\nabla^2 \mathbf{B} + \mu^2 \mathbf{B} = 0$ with the force-free constant μ,

$$\frac{B_z(\mathbf{r})}{B_{z0}} = J_0(\mu r) + CJ_1(\alpha r)\cos(\theta + kz) \tag{1}$$

$$\frac{B_\theta(\mathbf{r})}{B_{z0}} = J_1(\mu r) - \frac{C}{\alpha}\left[\mu J_1'(\alpha r) + \frac{k}{\alpha r}J_1(\alpha r)\right]\cos(\theta + kz) \tag{2}$$

$$\frac{B_r(\mathbf{r})}{B_{z0}} = -\frac{C}{\alpha}\left[kJ_1'(\alpha r) + \frac{\mu}{\alpha r}J_1(\alpha r)\right]\sin(\theta + kz). \tag{3}$$

Such a solution (dubbed the Freidberg solution) is obtained by truncating the infinite series and keeping the first two modes through a standard separation of variables procedure. For $C \equiv 0$, the solution reduces to the
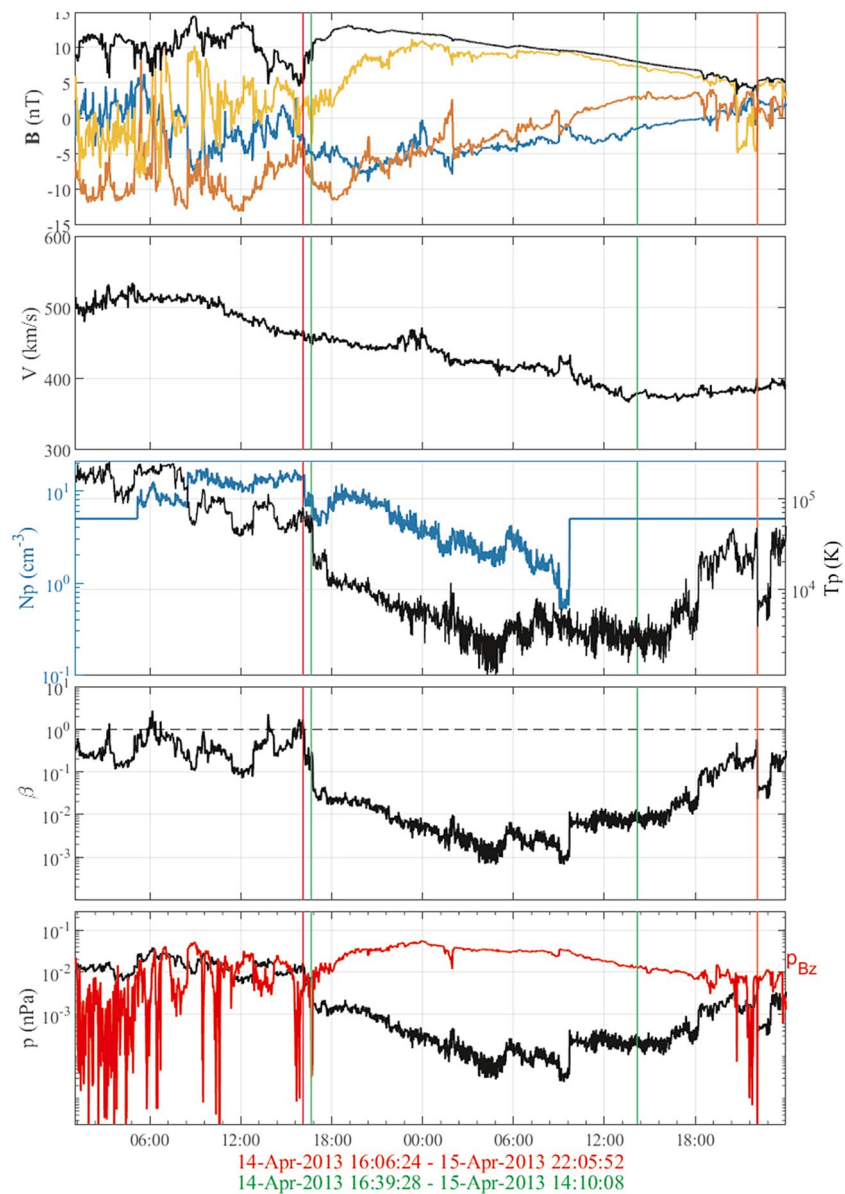
Figure 1. Time-series from the ACE spacecraft measurements for Case 1. From top to bottom: magnetic field components in R (blue), T (brown), and N (gold) coordinates, and magnitude (black), bulk speed, proton density (left axis) and temperature (right axis), proton β, and thermal and axial magnetic pressure (red). The vertical lines mark the intervals for the GS reconstruction (green) and the optimization analysis (red) of the Freidberg solution with the corresponding time periods denoted beneath the bottom panel, respectively. ACE, Advanced Composition Explorer; GS, Grad-Shafranov.

axisymmetric Lundquist solution, and the traditional Lundquist solution fitting to MCs ensues. Generally, the solution has 3D dependence on spatial dimensions, but it is also periodic in z with a period/wavelength $2\pi/k$, thus called a solution of "helical symmetry" with mixed helical states of azimuthal wavenumbers $m = 0$ and 1. The parameter C determines the amplitude of the $m = 1$ mode, which gives rise to the variation in θ. Following Freidberg (2014), the LFFF constant is denoted μ and the parameter $\alpha = (\mu^2 - k^2)^{1/2}$. The usual Bessel's functions of the first kind of the zeroth and first order are denoted J_0 and J_1, respectively. The Freidberg solution has 3D variations in that the cross section varies along the z dimension, which generally prohibits the appearance of a straight field line along z. Therefore, for a "flux rope" configuration represented by the Freidberg solution, the writhe will be present in the form of winding flux bundles in lack of a central straight field line.

$\chi^2 = 0.978$, $Q = 0.531$
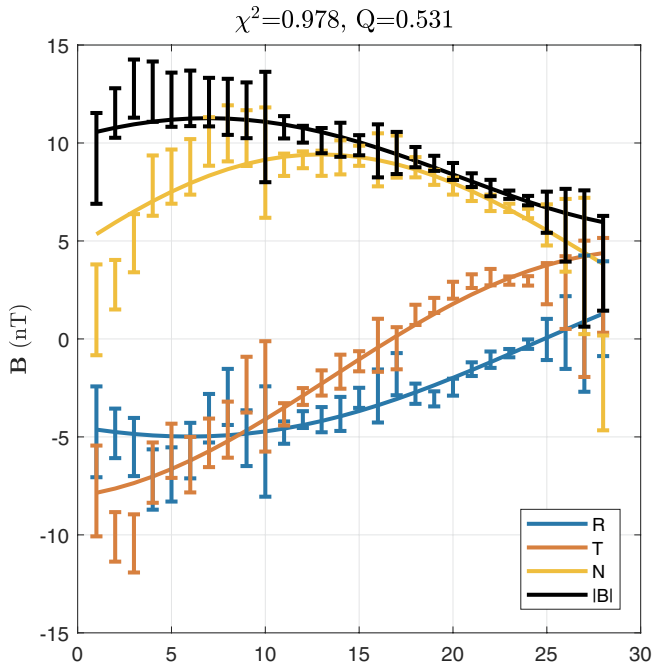
Figure 2. The optimal fitting results to the Freidberg solution for Case 1. The error bars are the ACE measurements with uncertainties in hourly averages, and the solid curves are the Freidberg solution, for the R, T, and N components, and the field magnitude, respectively, as indicated by the legend. ACE, Advanced Composition Explorer.

For an MC event detected in in situ spacecraft data, an interval is chosen for a χ^2 minimization process to determine the unknown parameters in the Freidberg solution, that is, Equations (1)–(3). A reduced χ^2 function is defined to assess the difference between the measured magnetic field components **b** and the analytic solution **B**, subject to underlying uncertainties:

$$\chi^2 = \frac{1}{\text{dof}} \sum_{v=X,Y,Z} \sum_{N}^{i=1} \frac{(b_{vi} - B_{vi})^2}{\sigma_i^2}. \qquad (4)$$

A minimum χ^2 value is sought for an interval with N magnetic field data points, often downsampled from 1-min cadence to 1 h. Then, the degree of freedom (dof) of the system is $3N-p-1$, with p the number of parameters to be optimized. According to Press et al. (2007), a quantity Q, indicating the probability of a value greater than the specific χ^2 value, is also obtained for reference. It is calculated by $Q = 1-\text{chi2cdf}(\chi^2, \text{dof})$, where the function chi2cdf is the cumulative distribution function of χ^2. The corresponding uncertainties σ are estimated by taking the root-mean-square variation of the underlying 1-min measurements over each 1-h interval, an approach adopted by the ACE Science Center MAG data processing (see http://www.srl.caltech.edu/ACE/ASC/level2/mag_l2desc.html). The set of main parameters to be optimized includes C, μ, k, the pair of the directional angles of the z axis, (δ, ϕ), together with additional geometrical parameters to allow for more freedom of the solution with respect to the spacecraft path. Simply put, besides that the z axis orientation is completely arbitrary, the outer cylinder enclosing the solution domain is allowed to translate along and perpendicular to, as well as to rotate about the z axis. This fully accounts for the 3D nature of the solution. Detailed descriptions of the algorithm will be reported elsewhere. In the following case studies, the parameters μ and k become dimensionless by multiplying a length scale R_0 which is the normalization constant for r and z.

3. Case Studies

We present two case studies to illustrate the method. Case 1 is an MC event observed on April 14–15, 2013 at 1 au. Figure 1 shows the time-series plot from the ACE spacecraft measurements. A typical MC structure is present with relatively strong field magnitude and rotating field components, and depressed proton β. Two intervals are marked. Both last for over 20 h. The average Alfvén Mach number in the reference frame moving with the MC structure is 0.23, and the average β is 0.01, justifying the assumption of quasi-static equilibrium and approximate force freeness. A GS reconstruction was performed with acceptable output. The optimization result for the Freidberg solution is shown in Figure 2 with the minimum reduced $\chi^2 = 0.978$ and $Q = 0.531$.

Table 1 lists the main fitting parameters for the two cases. The normalization constants for the length scale and the magnetic field are denoted by R_0 and B_{z0}. For the Freidberg solution, the parameter C indicates the contribution from the variations in the θ and z dimensions. The parameter k represents the wavenumber in the z dimension. Therefore, both the parameters C and k represent the 3D characteristics of the solution (for $C = 0$, the solution returns to the 1D Lundquist solution, while for $k = 0$, a 2D solution results). The force-free constant is given by μ and the sign of the parameter μ indicates the sign of magnetic helicity (i.e., the handedness or chirality). The z axis orientation is given by the polar and azimuthal angles (δ, ϕ) in radians in the RTN coordinates. The axial magnetic flux within the positive polarity region (where $B_z > 0$) on the cross section is denoted Φ_z.

Figures 3 and 4 further demonstrate the similarity, but more pronounced the differences between the two solutions. Figure 3, left panel, shows the cross section of a flux rope from the GS reconstruction in the form of the contour lines of the 2D flux function and the cospatial axial field. In other words, the solution is fully

Table 1
Optimal Fitting Parameters of the Freidberg Solution for the Two Case Studies From the ACE Spacecraft Measurements

MC interval (UT) hh:mm MM/DD/YY	R_0 (AU)	B_{z0} (nT)	C	μ	k	(δ, ϕ) (radians)	$\Phi_z(10^{20}$ Mx)
16:06 04/14/13 to 22:06 04/15/13		0.14	10.5	0.0367	−1.61	−1.60	(0.433, 2.13)
08:04 07/15/12 to 13:52 07/16/12	0.33	21.9	−2.27	5.64	−4.07	(0.867, 4.15)	36

represented by this 2D rendering in a view down the z axis of a set of (nested) distinct flux surfaces. It is readily seen that the flux rope configuration is left handed as indicated by the white arrows and the positive B_z field along the spacecraft path. On the other hand, the Freidberg solution, given to the right, loses this 2D feature. This is the same view down the z axis with the cross section drawn at $z = 0$ where the first point along the spacecraft path is located. Then, the spacecraft path (green dots) deviates from this plane. There are no distinct flux surfaces, and such a cross-section plot will change with z. Both solutions yield a unipolar region of positive axial field and are left handed. The axial magnetic flux is $\Phi_z = 5.7 \times 10^{20}$ Mx and 9.6×10^{20} Mx, respectively. For the Freidberg solution, the sign of the parameter $\mu = -1.61$ indicates the negative sign of magnetic helicity, that is, left-handed chirality. The larger amount of flux in the Freidberg solution is partially due to the corresponding larger interval used for this analysis (see Figure 1).

Figure 4 provides a 3D view of field-line configurations toward the Sun for both solutions. Overall, they are similarly oriented in space, with the z axes pointing mainly northward. The drastic difference, however, lies not in the number of field lines drawn for each, but in the intrinsic differences between a 2D and a (quasi-)3D configuration. In the right panel, more field lines are drawn to illustrate the overall winding of the flux rope body, which is not present in the left panel where the flux rope with a discernable central field line remains straight.

It is more informative to demonstrate by Case 2 the novelty of the new approach and the complexity of the field configuration represented by the Freidberg solution, whereas the GS reconstruction failed, mainly due to the failure in finding a reliable invariance direction $\hat{z}$ for a 2D configuration. Case 2 is a well-studied Sun-Earth connection event with a prolonged MC interval occurring on July 15–16, 2012. We refer readers to the VarSITI Campaign event webpage (http://solar.gmu.edu/heliophysics/index.php/07/14/2012_17:00:00_
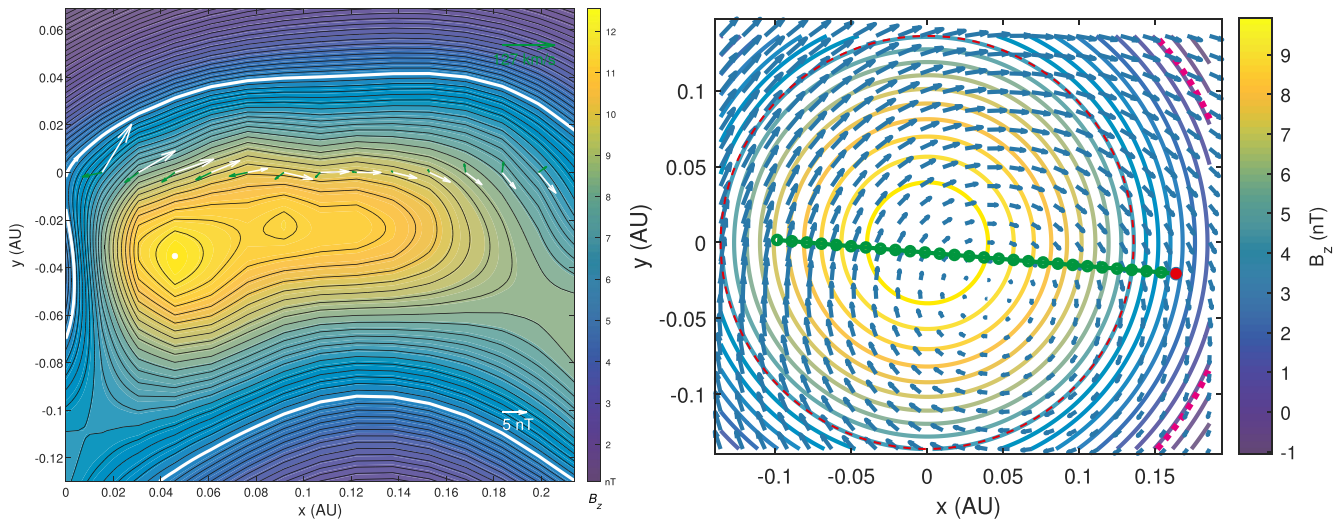
Figure 3. The cross sections of the GS reconstruction result (left panel), and the Freidberg solution at $z = 0$ (right panel) for Case 1. In the left panel, the black contour lines represent the transverse field lines and color represents the axial field with scales indicated by the colorbar. The white (green) arrows along $y = 0$ are the measured transverse field (remaining transverse flow) vectors along the spacecraft path. A reference vector for each set is shown (where the green reference vector is of the magnitude of the average Alfvén speed). In the right panel, the color contours show the axial field at $z = 0$, and the corresponding transverse field is shown by arrows. The dots mark the spacecraft path during the analysis interval in 1 h increment from start (the leftmost green dot) to the end (the red dot). Note that they are not lying on this plane except for the leftmost dot. GS, Grad-Shafranov.
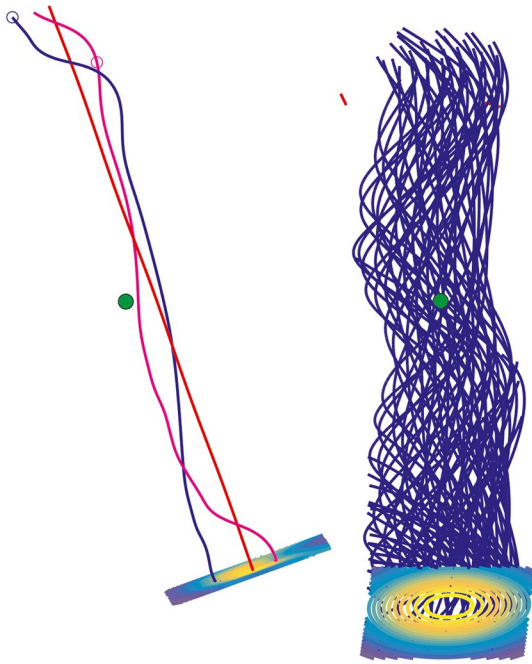
Figure 4. The 3D view toward the Sun of the field-line configurations for the GS reconstruction result (left panel), and the Freidberg solution (right panel), for Case 1. The big green dot marks the spacecraft path along the −R direction, the N direction is straight up, and the T direction is horizontally to the right. Both sets of field lines are winding upward out of the bottom plane where contours of B_z are shown. The z axis orientations are (0.08206, −0.3377, 0.9377) and (−0.4706, −0.0350, 0.8817), in RTN coordinates, respectively. GS, Grad-Shafranov.

UTC) for detailed information and references on relevant studies. An optimal Freidberg solution is obtained over a 27-h interval, as shown in the left panel of Figure 5. The reduced χ^2 value is slightly greater than 1. The corresponding set of optimal parameters is given in the third row of Table 1, indicating a more significant helical component ($|C| \gg 0$) and right-handed chirality ($\mu > 0$). Indeed, the corresponding 3D field-line configuration in Figure 5 (right panel) shows a striking double-helix structure with two bundles of field lines (blue and red) winding up and down along the z axis and around each other. The cross section at the bottom clearly shows the mixed B_z polarity regions next to each other, corresponding to the two flux bundles. Both are right handed. In this event, the spacecraft is taking a glancing path across such a complex system.

4. Summary

In summary, we have developed a new approach to model the MC magnetic field in a quasi-3D configuration. The model is based on an LFFF formulation presented in Freidberg (2014), which is a generalization of the well-known Lundquist solution. The solution is 3D in nature as a function of (r, θ, z) in a cylindrical coordinate system, but with periodicity in z. A χ^2 minimization process is devised by using the in situ spacecraft measurements with underlying uncertainty estimates to determine the optimal set of parameters that yields a solution with the best fit to the magnetic field vectors along the spacecraft path. Two case studies are presented to illustrate the merit of the methodology. Both results are obtained with minimum reduced $\chi^2 \approx 1$ and the associated $Q \gg 10^{-3}$, deemed acceptable according to Press et al. (2007). Case 1 exhibits a flux rope configuration with certain similarity to the corresponding 2D GS reconstruction result. Their z axis orientations and the axial magnetic flux contents are similar, and the chirality is the same. However, the results
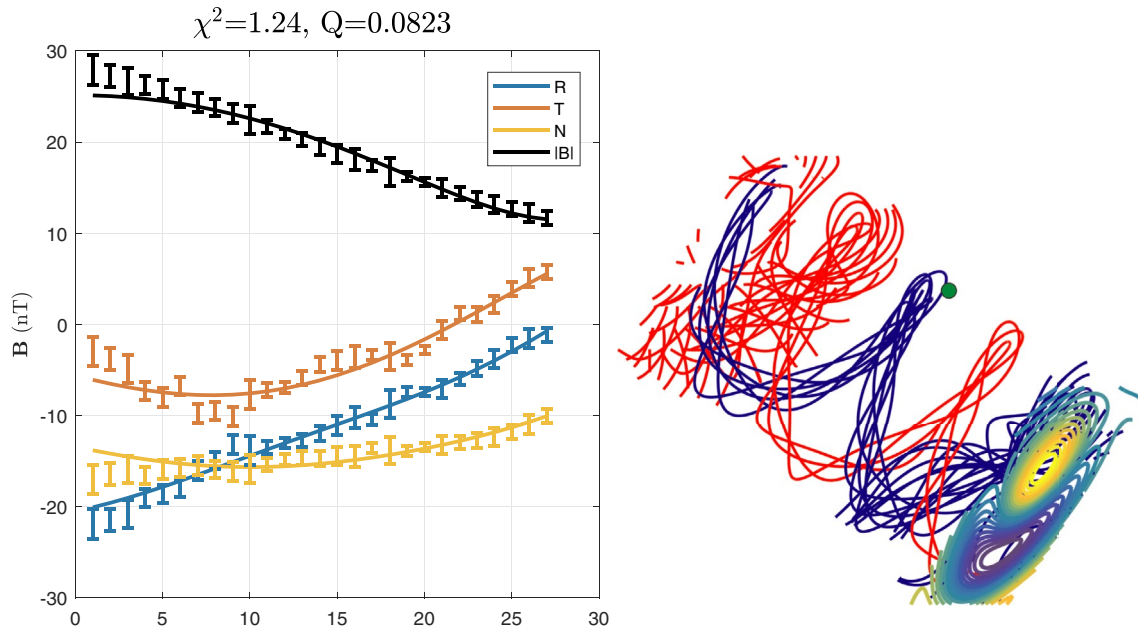
Figure 5. Left panel: The optimal fitting result to the Freidberg solution for Case 2. The format is the same as Figure 2. Right panel: The 3D view toward the Sun of the field-line configuration for the Freidberg solution. The format is the same as Figure 4. The set of red field lines are winding downward into the bottom plane. The z axis orientation is (−0.3265, −0.7509, 0.5741) in the RTN coordinates.

are markedly different in that the Freidberg solution exhibits a more general and intrinsically 3D field configuration with a winding flux rope body. Potentially, more complex MC structure is revealed by Case 2 in which a double-helix configuration is obtained. The cross section of the structure contains two adjacent regions of opposite field polarities (so are the currents) where the two helical flux bundles originate, both with right-handed chirality. Such a configuration, originating from the Sun, implies that the foot point regions must have mixed polarities as well. The ultimate proof of these implications has to come from quantitative comparisons with solar source region properties. This future investigation involving more extensive lists of events with well-coordinated observations will be facilitated by this new tool developed here, complementary to the existing ones, and will be pursued within our team.

Data Availability Statement

The ACE spacecraft merged magnetic field (MAG) and the solar wind electron, proton, and alpha monitor (SWEPAM) Level 2 data are publicly available via the ACE Science Center (http://www.srl.caltech.edu/ACE/ASC/level2/lvl2DATA_MAG-SWEPAM.html).

References

Al-Haddad, N., Roussev, I. I., Möstl, C., Jacobs, C., Lugaz, N., Poedts, S., & Farrugia, C. J. (2011). On the internal structure of the magnetic field in magnetic clouds and interplanetary coronal mass ejections: Writhe versus twist. *The Astrophysical Journal Letters*, *738*, L18. https://doi.org/10.1088/2041-8205/738/2/L18

Amari, T., Canou, A., Aly, J.-J., Delyon, F., & Alauzet, F. (2018). Magnetic cage and rope as the key for solar eruptions. *Nature*, *554*(7691), 211–215. https://doi.org/10.1038/nature24671

Berger, M. A., & Field, G. B. (1984). The topological properties of magnetic helicity. *Journal of Fluid Mechanics*, *147*, 133–148. https://doi.org/10.1017/S0022112084002019

Duan, A., Jiang, C., He, W., Feng, X., Zou, P., & Cui, J. (2019). A study of pre-flare solar coronal magnetic fields: Magnetic flux ropes. *The Astrophysical Journal*, *884*(1), 73. https://doi.org/10.3847/1538-4357/ab3e33

Farrugia, C. J., Janoo, L. A., Torbert, R. B., Quinn, J. M., Ogilvie, K. W., Lepping, R. P., et al. (1999). A uniform-twist magnetic flux rope in the solar wind. In S. T., Suess, G. A., Gary, & S. F., Nerney (Eds.), *American institute of physics conference series* (Vol. 471, pp. 745–748). Melville, NY: American Institute of Physics (AIP) Publishing. https://doi.org/10.1063/1.58724

Freidberg, J. P. (2014). *Ideal mhd* (pp. 546–547). Cambridge, UK: Cambridge University Press.

Hu, Q. (2017). The Grad-Shafranov reconstruction in twenty years: 1996–2016. *Science China Earth Sciences*, *60*, 1466–1494. https://doi.org/10.1007/s11430-017-9067-2

Hu, Q., Qiu, J., Dasgupta, B., Khare, A., & Webb, G. M. (2014). Structures of interplanetary magnetic flux ropes and comparison with their solar sources. *The Astrophysical Journal*, *793*, 53. https://doi.org/10.1088/0004-637X/793/1/53

Hu, Q., Smith, C. W., Ness, N. F., & Skoug, R. M. (2003). Double flux-rope magnetic cloud in the solar wind at 1 AU. *Geophysical Research Letters*, *30*(7), 1385. https://doi.org/10.1029/2002GL016653

Hu, Q., Smith, C. W., Ness, N. F., & Skoug, R. M. (2004). Multiple flux rope magnetic ejecta in the solar wind. *Journal of Geophysical Research*, *109*, 3102. https://doi.org/10.1029/2003JA010101

Hu, Q., & Sonnerup, B. U. Ö. (2001). Reconstruction of magnetic flux ropes in the solar wind. *Geophysical Research Letters*, *28*, 467–470. https://doi.org/10.1029/2000GL012232

Hu, Q., & Sonnerup, B. U. Ö. (2002). Reconstruction of magnetic clouds in the solar wind: Orientations and configurations. *Journal of Geophysical Research*, *107*(A7), 1142. https://doi.org/10.1029/2001JA000293

Jiang, C., Wu, S. T., Feng, X., & Hu, Q. (2016). Data-driven magnetohydrodynamic modelling of a flux-emerging active region leading to solar eruption. *Nature Communications*, *7*, 11522. https://doi.org/10.1038/ncomms11522

Lundquist, S. (1950). On force-free solution. *Arkiv för Fysik*, *2*, 361.

Nieves-Chinchilla, T., Jian, L. K., Balmaceda, L., Vourlidas, A., dos Santos, L. F. G., & Szabo, A. (2019). Unraveling the internal magnetic field structure of the Earth-directed interplanetary coronal mass ejections during 1995–2015. *Solar Physics*, *294*(7), 89. https://doi.org/10.1007/s11207-019-1477-8

Nieves-Chinchilla, T., Linton, M. G., Hidalgo, M. A., Vourlidas, A., Savani, N. P., Szabo, A., et al. (2016). A circular-cylindrical flux-rope analytical model for magnetic clouds. *The Astrophysical Journal*, *823*, 27. https://doi.org/10.3847/0004-637X/823/1/27

Nieves-Chinchilla, T., Vourlidas, A., Raymond, J. C., Linton, M. G., Al-haddad, N., Savani, N. P., & Hidalgo, M. A. (2018). Understanding the internal magnetic field configurations of ICMEs using more than 20 years of wind observations. *Solar Physics*, *293*(2), 25. https://doi.org/10.1007/s11207-018-1247-z

Osherovich, V. A., Fainberg, J., & Stone, R. G. (1999). Multi-tube model for interplanetary magnetic clouds. *Geophysical Research Letters*, *26*, 401–404. https://doi.org/10.1029/1998GL900306

Press, W. H., Teukolsky, S. A., Vetterling, W. T., & Flannery, B. P. (2007). *Numerical recipes in C++: The art of scientific computing* (p. 778). New York, NY: Cambridge University Press. http://numerical.recipes/

Qiu, J., Hu, Q., Howard, T. A., & Yurchyshyn, V. B. (2007). On the magnetic flux budget in low-corona magnetic reconnection and interplanetary coronal mass ejections. *The Astrophysical Journal*, *659*, 758–772. https://doi.org/10.1086/512060

Vourlidas, A. (2014). The flux rope nature of coronal mass ejections. *Plasma Physics and Controlled Fusion*, *56*(6), 064001. https://doi.org/10.1088/0741-3335/56/6/064001

Vourlidas, A., Lynch, B. J., Howard, R. A., & Li, Y. (2013). How many CMEs Have Flux Ropes? Deciphering the signatures of shocks, flux ropes, and prominences in coronagraph observations of CMEs. *Solar Physics*, *284*(1), 179–201. https://doi.org/10.1007/s11207-012-0084-8

Wang, W., Liu, R., Wang, Y., Hu, Q., Shen, C., Jiang, C., & Zhu, C. (2017). Buildup of a highly twisted magnetic flux rope during a solar eruption. *Nature Communications*, *8*, 1330. https://doi.org/10.1038/s41467-017-01207-x

Wang, Y., Zhuang, B., Hu, Q., Liu, R., Shen, C., & Chi, Y. (2016). On the twists of interplanetary magnetic flux ropes observed at 1 au. *Journal of Geophysical Research: Space Physics*, *121*(10), 9316–9339. https://doi.org/10.1002/2016JA023075

Wang, W., Zhu, C., Qiu, J., Liu, R., Yang, K. E., & Hu, Q. (2019). Evolution of a magnetic flux rope toward eruption. *The Astrophysical Journal*, *871*(1), 25. https://doi.org/10.3847/1538-4357/aaf3ba

Zhu, C., Qiu, J., Liewer, P., Vourlidas, A., Spiegel, M., & Hu, Q. (2020). How does magnetic reconnection drive the early-stage evolution of coronal mass ejections? *The Astrophysical Journal*, *893*(2), 141. https://doi.org/10.3847/1538-4357/ab838a